INVESTIGATIONS ON THE ELECTRICAL, THERMAL AND THIRD ORDER NONLINEARITY OF ALLYLTHIOUREA CADMIUM CHLORIDE (*ATCC)* SINGLE CRYSTALS

Sreekanth G[1], Santhoshkumar R[2], Ginson P. Joseph[3*]

Abstract
Single crystals of Allylthiourea Cadmium Chloride (ATCC), organometallic nonlinear optical material have been grown from aqueous solution by slow evaporation method. The structure of the grown single crystals have confirmed by single crystal XRD and CHN whereas the morphology has been studied using SEM. The optical transparency and optical band gap of the grown crystal are determined using UV-Vis spectroscopy. The third order nonlinear optical property of the ATCC is studied using Z-scan technique. The dielectric properties and ac conductivity of the crystal as a function of frequency and temperature are also investigated.

Keywords: Single crystal; Scanning Electron Microscopy; Z-scan; Dielectric properties

[1]Department of Basic Science and Humanities, Muthoot Institute of Technology and Science, Kerala – 682308, India
[2]Department of Physics, St. George's College, Aruvithura, Kerala- 686122, India
[3]*Department of Physics, St. Thomas College, Palai, Kerala 686574, India

***Corresponding Author:** Ginson P. Joseph
*Department of Physics, St. Thomas College, Palai, Kerala 686574, India Tel.: +919447064652,
E-mail: ginsonpj@gmail.com

DOI: 10.53555/ecb/2021.10.1.03

1. Introduction

Highly optical nonlinear materials are attracting a great deal of attention because of their applications in the field of photonics especially in optical switches, optical modulators, electro-optical devices, optical disk data storage, laser driven fusion, laser remote sensing etc.[1,2]. Studies of organometallic complexes have shown that nearly formed co-ordination compound can strengthened the interaction between the molecules and thus improving the mechanical properties [3-5]. Unique charge transfer transitions is an important aspect of utilizing these materials for nonlinear optics; either from metal to ligand or from ligand to metal. Because of this, the metal–ligand bonding is expected to display large molecular hyperpolarize ability in semiorganic materials, due to the transfer of electron density between the metal atom and the conjugated ligand system. With the assistance of this theory, many metal–organic coordination materials with good optical qualities have been designed and synthesized. Thiourea complexes which have low ultraviolet cut-off wavelengths, applicable for high power frequency conversion have received much attention.

ATMX (AT=allylthiourea, M=Cd, Hg, Cl or Br) are a series metal organic compound crystals with AT act as ligand [6]. An enhanced optical non linearity in the Allylthiourea complexes comes from the distortion of the tetrahedral, which is formed from three allylthiourea ($C_4H_8N_2S$, AT) and chlorine (Cl) or bromine (Br) combining with cadmium (Cd) or mercury (Hg). The present chapter deals with the growth and characterization of ATCC single crystals. Allylthioure cadmium chloride (ATCC) can be grown from aqueous solutions at moderate temperatures by adjusting the pH value range from 2.5to 5.

The low cut-off (285 nm) and widest transparent wave band (300 – 1500 nm) [7] of the Allylthiourea Cadmium Chloride (ATCC) crystal fascinated the chineese scientist and the ATCC crystal was first grown by Zhang et al in 1990 using slow cooling method. The investigations on the thermal properties done by by Zhang et [8] verified that ATCC has no water of crystallization and it is thermally stable upto 194 °C. The thermal expansion coefficient along c-axis is nearly three times that along the a-axis is verified by Sun et al [9]. Some non linear optical studies of the ATCC crystals were conducted and the optical parameters like non linear coefficient, refractive index and laser damaged threshold were already reported [10-12].

The present paper deals with synthesis, growth and characterizations of Allylthiourea Cadmium Chloride crystals.

2. Synthesis and Growth of ATCC crystals

ATCC was prepared by dissolving allylthiourea and cadmium chloride as the raw materials (purity>98%) in the molar ratio 3:1. The reaction to be takes place according to the following chemical equation

$$3CH_2 = CHCH_2NHCSNH_2 + CdCl_2 \rightarrow CdCl_2 (CH_2=CH\ CH_2NHCSNH_2)_3$$

The salt was mixed thoroughly and was dissolved in Millipore water having conductivity with continuous stirring. The stirring was continued for 6 hours and the pH of the solution was measured periodically. The temperature of the mixed solution was slowly increased and kept it below 60^0c. The saturated solution was filtered twice using a high quality watsman filter paper. The pH value of the solution was maintained between 3 and 4 by adding HCl [11]. The saturated mother solution was poured into a vessel and tightly closed with perforated cover. The solution was allowed to evaporate by putting small holes on the top of the cover. The very next day tiny crystals were formed by spontaneous nucleation. After few days defect free crystals with good shape have chosen for further growth. The defect free crystals hung in the mother solution using nylon thread for further growth. The colorless single crystals of ATCC with dimension 12 x 12 x 6 mm^3 were harvested within a period of three weeks. The solubility curve of the ATCC crystal is shown in the Fig.1. The photograph of good quality single crystals of ATCC is shown in Fig.2.

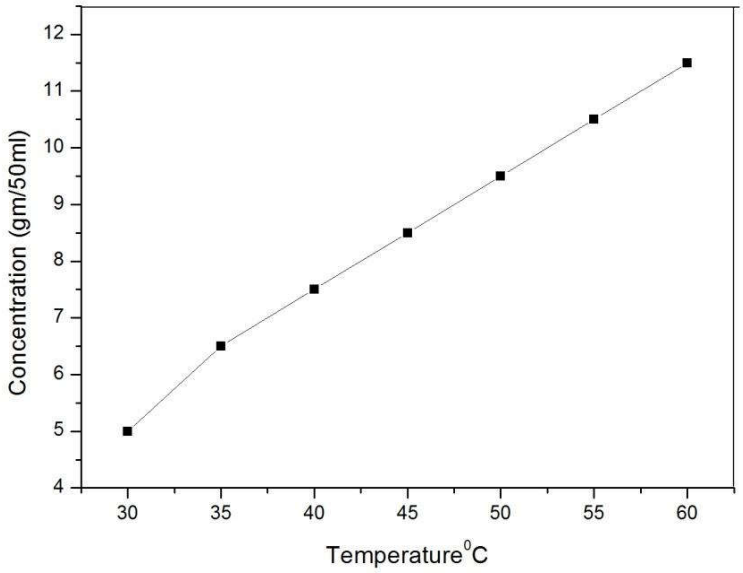

Fig.1: *Solubility curve of ATCC*

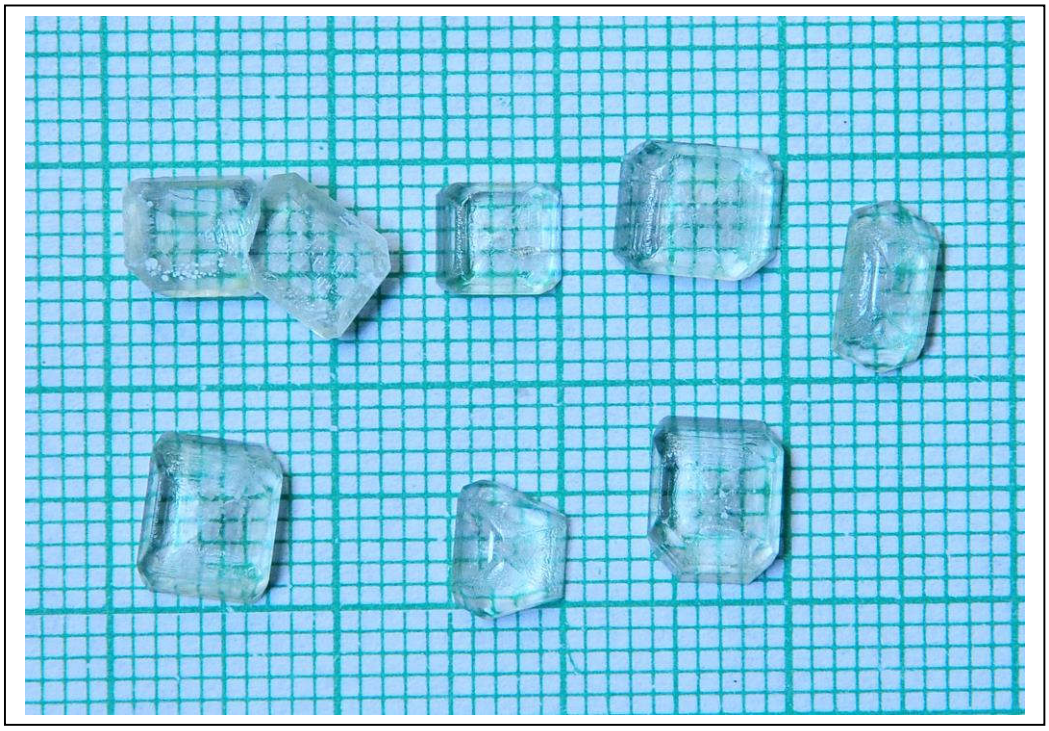

Fig.2: *Photograph of ATCC crystals*

3. Result and Discussion

3.1 Single crystal X-ray diffraction studies

Single crystal x ray diffraction studies reveals that ATCC crystals are belongs to Trigonal crystal system with $R3_C$ space group. The unit cell parameters are measured to be a = 11.491Å, b=11.491 Å, c= 27.900 Å, α=β=90^0, γ=120^0 and the cell volume V=3047 Å^3. The measured values are in well agreement with other papers published earlier [10-12].

3.2 CHN Analysis

Elemental analysis of the ATCC single crystals has been studied using ElementarVario El III Elemetal analyzer. Using the ATCC crystal formula, CdCl2 (CH2 = CHCH2NHCSNH2)3 molecular component (C, H, N) were theoretically calculated and compared it with experimental data. The data confirm the formation of the grown ATCC crystal which is given in the Table 1.

Table 1: *CHN Analysis*

Weight Composition %					
Carbon		**Hydrogen**		**Nitrogen**	
Theoretical	**Experimental**	**Theoretical**	**Experimental**	**Theoretical**	**Experimental**
27.09	27.08	4.55	4.49	15.80	15.83

3.3 FTIR Analysis of ATCC

FT-IR spectrum of ATCC (Fig.3) has been recorded between 400 and 4000 cm^{-1} to identify the functional groups present in the sample. The sharp intense peak is at 3437 cm^{-1} corresponds to the NH stretching of the amide group. The observed 1060 cm^{-1} which corresponds to ν(CN) stretching frequency and it is shifted to higher wave number when compared to the corresponding frequency found in the ligand compound allylthiourea (1543 cm-1). The band observed at 789 cm^{-1} is assigned to the bending vibration of C=S group. It reveals that the metal ion ($Cd2^{+)}$ coordinated only with sulphur that is present in AT [13]. The observed bands are given in the Table 2.

Table 2 *Assignments of the main FT-IR bands of ATCC*

Wave number cm^{-1}	Assignment
3437	ν NH_2
1622	δ(NH2)
789	ν (C=S)
990	*π*(CH)
1570	*ν*(CN), *δ*(NCN), *ν*(C S)

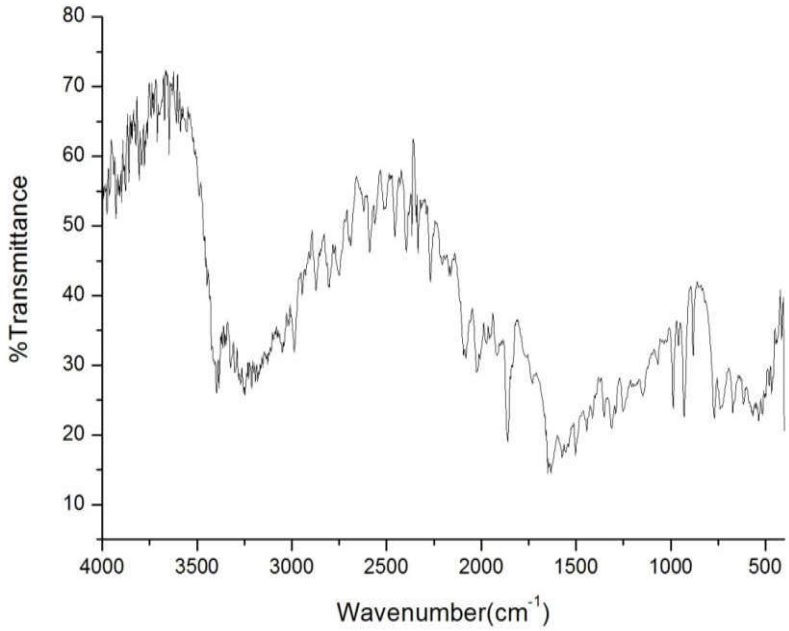

Fig. 3: *FTIR spectrum of ATCC crystals*

3.4 Scanning Electron Microscope (SEM)

The periodical arrangement of atoms is the characterizing property that makes crystals a unique class in the wide variety of solid groups. For to study the surface morphology of the grown crystals of ATCC the photograph of SEM pictures (Fig.4a - 4c***)*** were recorded with a magnification factors 1500, 5000, 10000 in the operating voltage of 20kV using JEOL JSM-6390 LV scanning electron microscope. The stacking of fundamenal units which is essential for a crystalline nature is evident from the photographs.

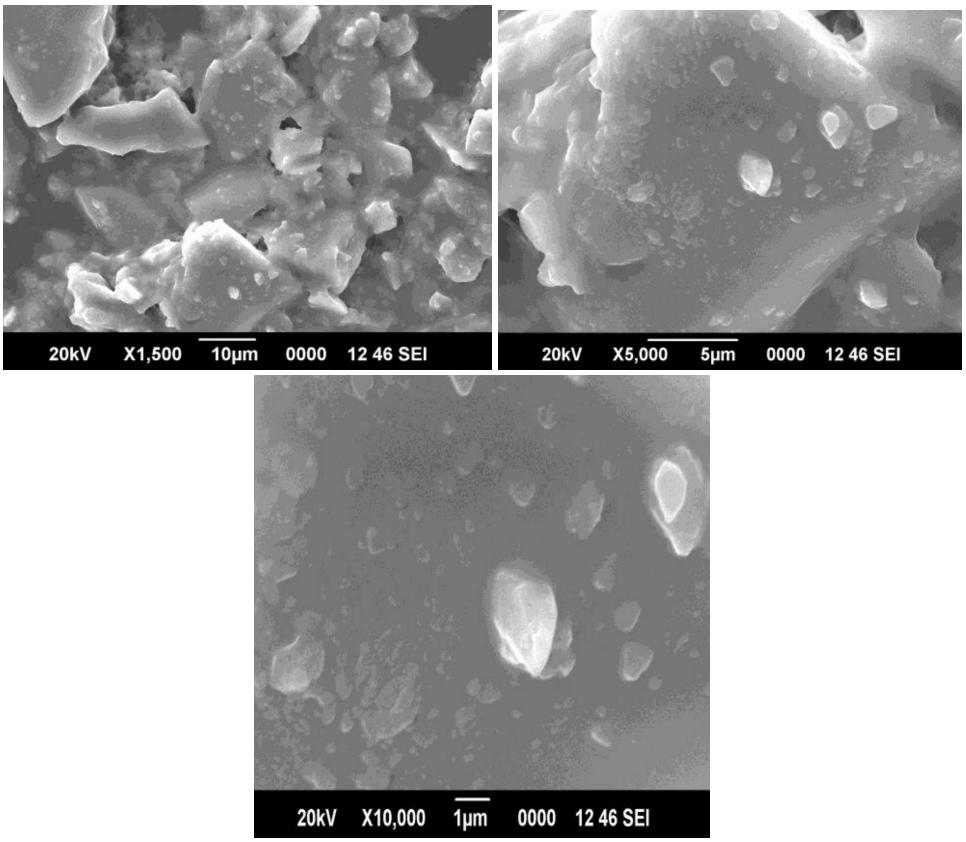

Fig. 4a - 4c: *SEM image of ATCC for different magnifications*

3.5 Thermal studies of ATCC

Thermogravimetric analysis (TGA) and differential thermal analysis (DTA) were carried out for the grown ATMC crystals by PerkinElmer STA6000. Thermal parameters has been recorded in the temperature range 40-700^0 at a rate of 10^0/min in inert nitrogen atmosphere is shown in Fig.5.The melting point of ATCC at 113.36^{0}C. The curve reveals that ATMC crystals are stable up to 228^{0}C.This is comparable to previously reported thermal analysis of the allylthiourea cadmium chloride crystals [14]. The thermal stability and melting points of the ATCC crystals are seems to be higher that of its ligand allylthiourea [15].

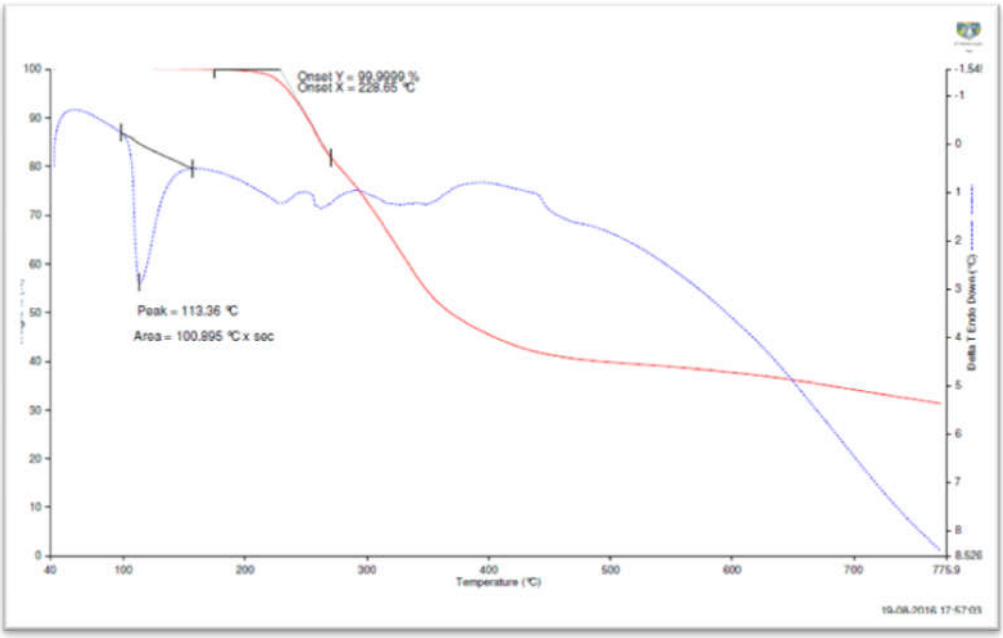

Fig.5: *Thermal analysis of ATCC crystals*

3.6 Optical absorption studies

The optical absorption spectrum of ATCC crystal has been taken in the wavelength ranging from 190-1100nm, and is shown in Fig.6. The UV cut-off wavelength is measured to be 290nm. The optical band gap of the ATCC crystal is determined using Tauc's relation[16], $\alpha h\nu = A (h\nu - E_g)^{n/2}$ where the E_g is the energy gap, A is a constant which is different for different transitions, a graph has been plotted between incident photon energy ($h\nu$) and $(\alpha h\nu)^2$ to determine the direct band gap value, where α is absorption coefficient. From the Tauc's plot (Fig.7), the band gap is estimated as 3.6eV by extrapolating the linear portion of the curve to zero absorption. The wide band gap of crystal is an indication of the large transmittance in the visible region [17]. The urbatch energy was measured to be 0.048eV by plotting a graph between photon energy versus ln α as shown in Fig.8.

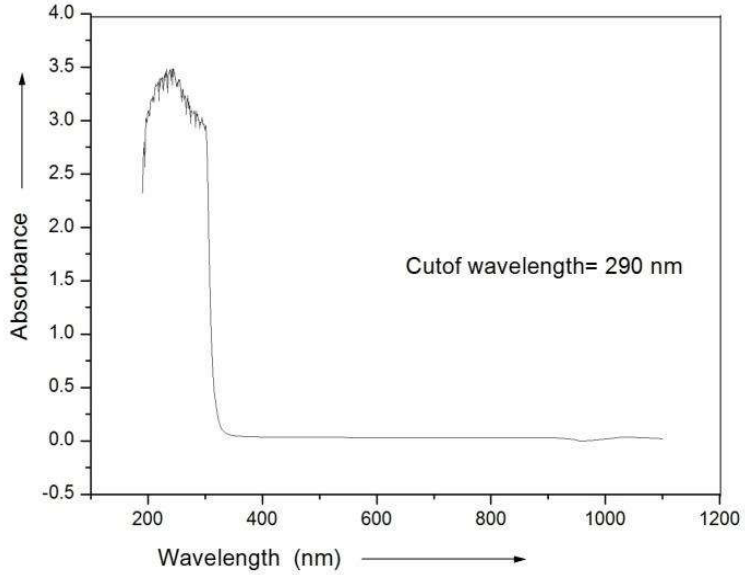

Fig.6: *Absorbance versus Wavelength graph of ATCC crystal*

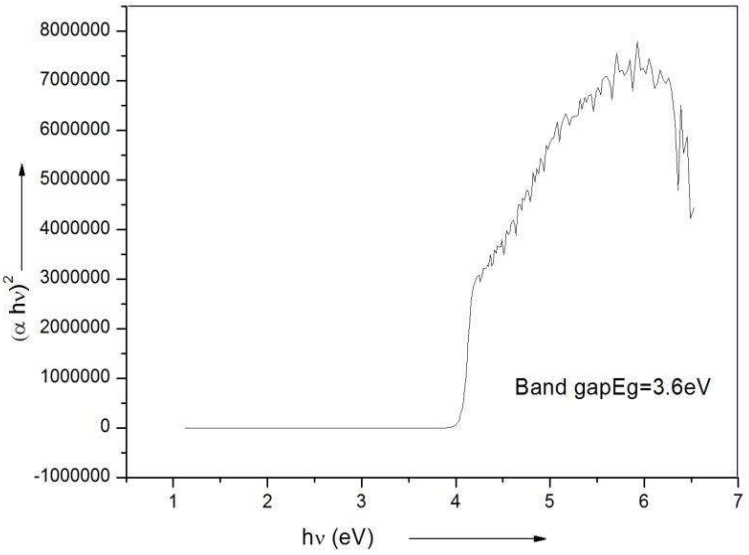

Fig.7: *Tauc's plot of ATCC crystal*

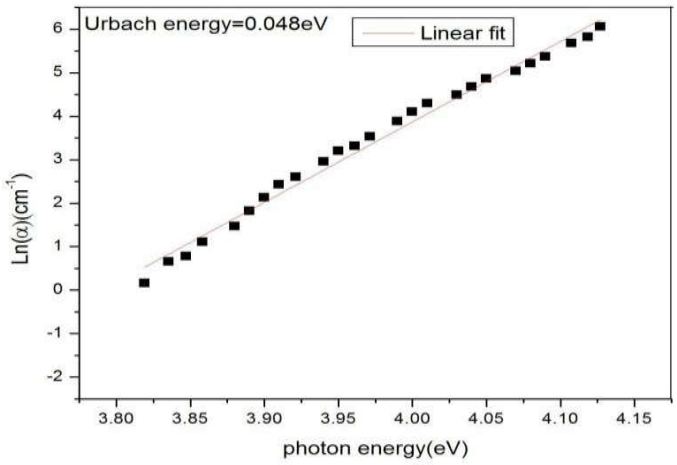

Fig.8: *The dependence of lnα with incident photon energy*

3.6 Electrical Studies

Good quality single crystal of ATCC with an area of 16 mm^2 was selected for dielectric studies and polished with high quality silver paste to avoid electrical contact. Dielectric constant Єr expresses the electric properties of the medium is calculated from the following equation, $Є_r = Ct / Є_0A$, where $Є_0$ is the permittivity of free space, t is the thickness of the sample and A is the area of cross section of the sample. Dielectric parameters give the information on how the interaction between molecules in the crystal takes place**.** The values of dielectric constant and dielectric loss in the frequency range 100Hz to 2MHz were obtained from the Agillent E4980 LCR meter. The real part of the dielectric constant is also plotted at the temperature range 75-90^0 C and it is found to be a very high dielectric constant ~550 at a temperature of about 90^0C(Fig.9). The crystals with high dielectric constant lead to power dissipation [18]. The large value of dielectric constant at low frequency is due to the presence of space charge polarization [19]. But at high frequencies, orientation polarization terminates, and hence the energy need not be worm out to rotate dipoles, as a result dielectric constant decreases; or the graph of dielectric constant versus frequency shoes an exponential decrease. The amount of power losses in a dielectric under the action of the alternating voltage applied to it is commonly known as dielectric loss. When an electric field oscillates, the dipoles in the system tend to follow the field, flipping back and forth as the field reverses its direction during each cycle. A dipole experiences some friction due to its collision with other molecule in the system. Or some energy is absorbed from the field, which is known as the dielectric loss, or it gives the information on how the interaction between molecules in the crystal takes place. The dielectric loss is measured from the Agillent E4980 LCR meter, and plotted with frequency in the range 100Hz to 2MHz in the temperature range 70-95^0C with an interval of 5^0C (Fig.10), and it is observed that at low frequencies the dielectric loss is moderately very high.

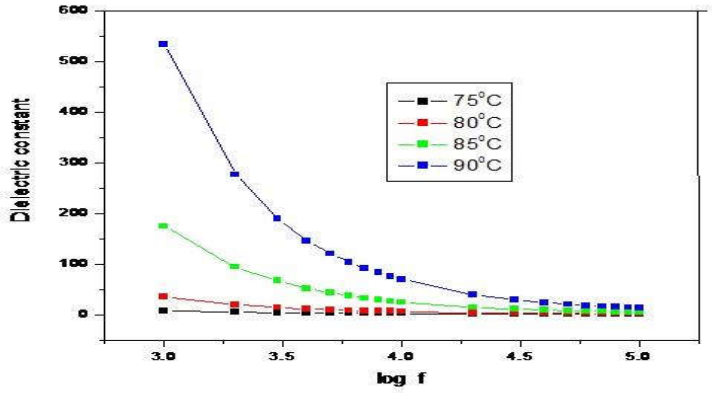

Fig. 9: *Log frequency versus Dielectric constant*

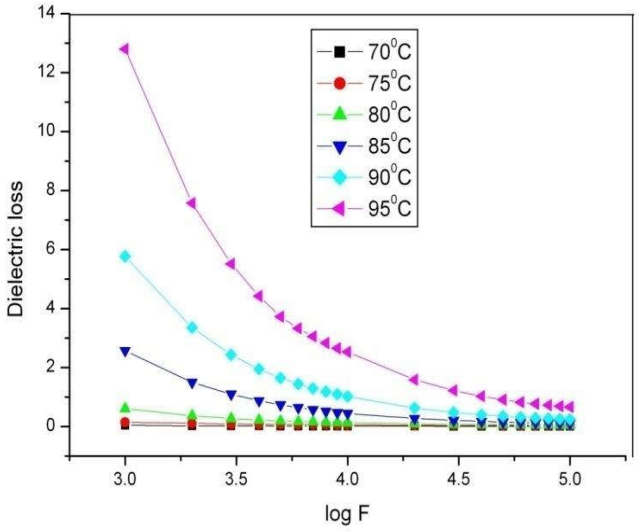

Fig.10: *Log frequency versus Dielectric loss*

The ac conductivity studies were also done with the above Agillent E 4980 LCR meter. The ac conductivity (σ) of the ATCC sample was calculated using the relation, $\sigma = 2\pi f\varepsilon_0\varepsilon_r \tan\delta\ \Omega^{-1}$ cm^{-1}. The graph of logarithmic conductivity with logarithmic frequency in the temperature range 70-95^{0}C is having a positive slope and is found to increase with frequency, at all temperatures where observations are made (Fig.11). The increase in conductivity could be attributed to reduction in space charge polarization at higher frequencies [20]. The electrical conductivity shows a linear relation when it is plotted against 1000/T at frequency 1kHz (Fig.12). This is an indication of the increase of conductivity with temperature. The Arrhenius plot (Fig.13), 1000/T and log (σT), is linear or it obey the Arrhenius equation $\sigma=\sigma_0\exp(E_a/k_BT)$. Where σ_0 is the pre-exponent factor, E_a is the activation energy for the conduction process and k is the Boltzmann constant.

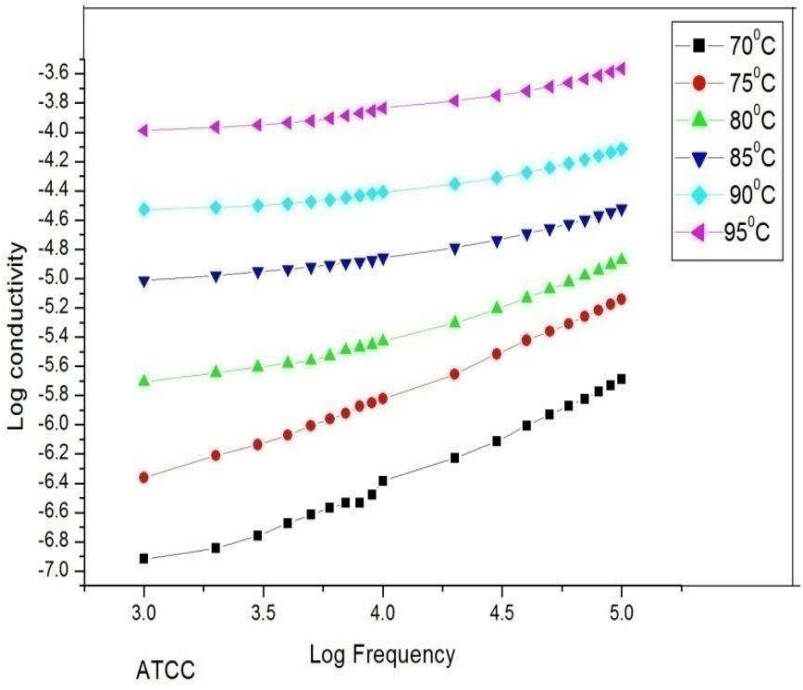

Fig. 11: *Log frequency versus Log conductivity of ATCC*

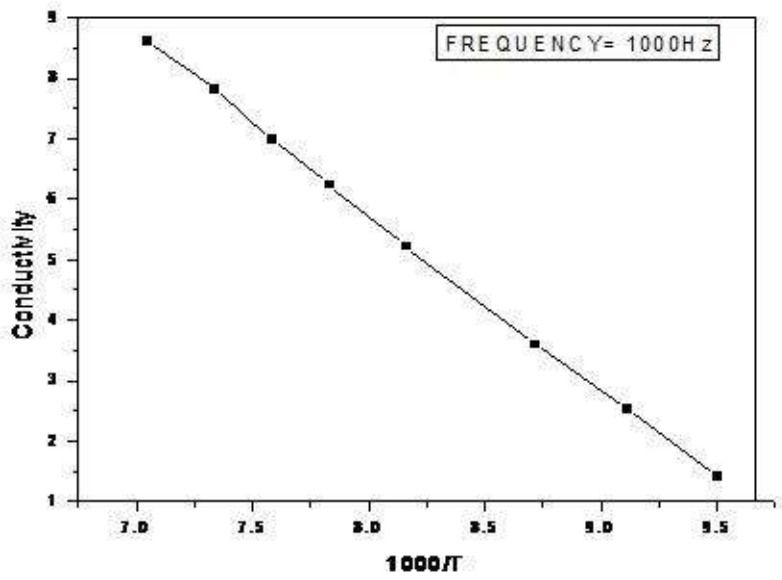

Fig.12: *1000/T versus Log conductivity of ATCC*

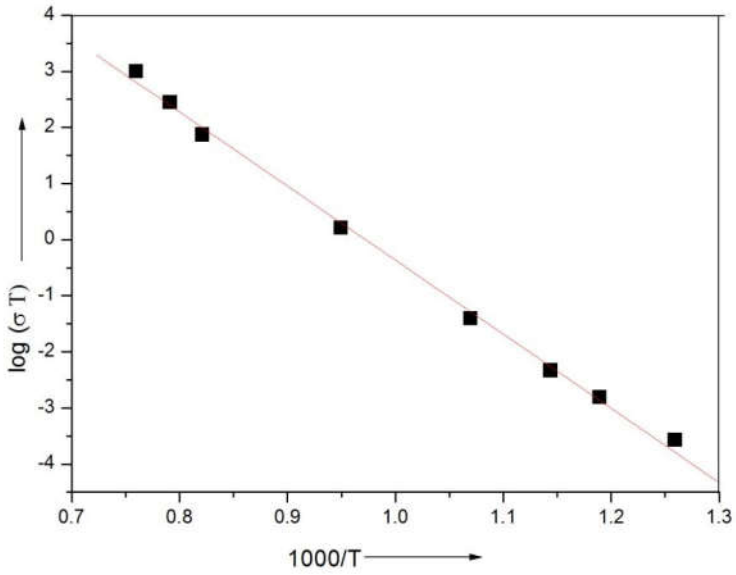

Fig.13: *Logarithm of (temperature X conductivity) versus 1000/T (Arrhenius plot)*

3.7 Piezoelectric studies

In noncentrosymmetric crystals, mechanical straining of a material produces an internal electric field, and vice versa. This property of the material is applicable in transducers which coverts mechanical energy into electrical energy and vice versa. Piezoelectric crystals are applicable in the field of laser technology and modern optical communication. Laser cavity length can be controlled by applying voltage to a piezoelectric crystal. The piezoelectric charge coefficient (d_{33} pC/N) of the ATCC crystal has been measured by using a Piezometer system in the frequency range 50-500Hz and applying a tapping force of 0.25N at 25^0C.The experimental data's are given in the Table 3.

Table 3. *Piezoelectric charge coefficient determination*

Sample	Thickness of ATCC sample (mm)	Tapping Frequency	Tapping force	Piezoelectric charge coefficient
ATCC	1.4	50-300 MHz	0.25 N	6 pc/N

P-E loop for a substance is a plot of polarization (P) developed, against the electric field applied to that device (E) at a given frequency. The Piezoelectric hysteresis loop, of the ATCC crystal is shown in Fig.14. Piezoelectric Hysteresis loop parameters such as remnant polarization (P_r), and maximum polarization are determined. The measured values are given in the Table.4. A corona dc poling technique is employed to the shaped ATCC crystal, but also after poling the values of P_r & E_c remains unaffected as an indication of saturation of dipoles.

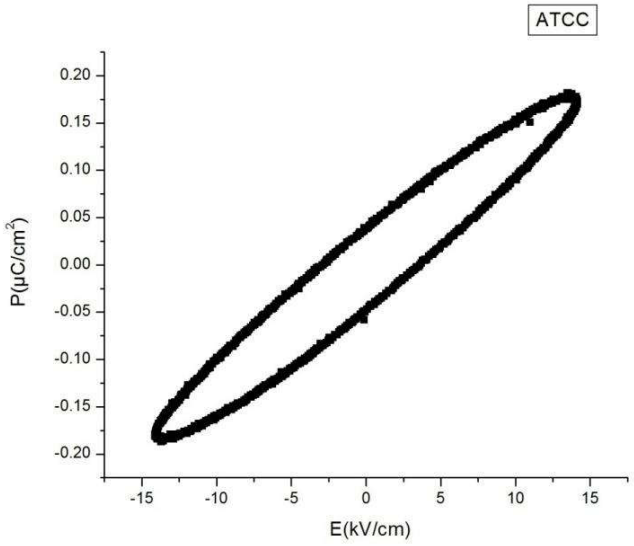

Fig. 14: *PE loop of ATCC crystal*

Table: 4 *Hysteresis loop parameters of ATCC crystal*

Sample	Remnant polarization (P_r) ($\mu C/cm^2$)	Coercive field (E_c) (kV/cm)	Maximum Electric field E_{max} kV/cm	Maximum Polarization P_{max} (($\mu C/cm^2$)
ATCC	**0.043**	**3.262**	**14.140**	**0.185**

3.8 Photoconductivity studies

Using the Keithley 6485 Picoammeter the photoconductivity measurement was done. The dark current was recorded by keeping the sample unexposed to any radiation. The experiment was performed at room temperature (305 K). The applied field was varied from 0 to 400 V/cm. For measuring the photo current, the sample was

lluminated with a mercury lamp of 80W power by focusing a spot of light to the sample with the help of a converging lens. The resulting photo current is measured by varying the applied field for the same range. The observation values are tabulated in the Table 5. The variations of photo current (Ip) and dark current (I_d) with applied field are plotted in Fig.15. As expected the plot of dark current is always higher than the photocurrent for different applied field which is said to exhibit negative photoconductivity. The negative photoconductivity exhibited by the sample may be due to the reduction in the number of charge carriers or their life time, which is explained by Stockman model [21].

Table: 5 Photo conductivity data of ATCC

Electric field (E) (V/cm)	**Dark current (I_d) (nA)**	**Photo current (I_p) (nA)**
20	0.315	0.312
40	0.624	0.601
60	0.967	0.921
80	1.331	1.111
100	1.654	1.414
120	2.064	1.914
140	2.442	2.121
160	2.902	2.714
180	3.274	3.144
200	3.602	3.414

220	3.871	3.701
240	4.235	4.134
260	4.634	4.544
280	4.926	4.825
300	5.002	4.914
320	5.212	5.021
340	5.792	5.55
360	6.024	5.914

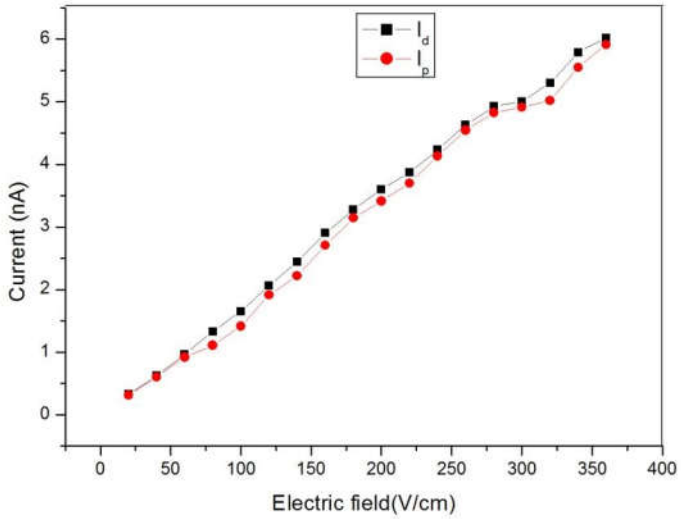

Fig.15: *The variations of photo current and dark current with applied field*

3.9 Z scan studies of ATCC

Open aperture Z-scan technique of ATCC crystals were carried out using laser pulses of 5 nanosecond duration (λ=532 nm, Nd: YAG laser), for the optical nonlinearity measurements [22]. In the Z-scan experiment, a laser beam is first focused using a lens, and the direction of beam propagation is taken as the z-axis. The focal point is taken as z = 0, so that the sign of z is negative on one side and positive on the other. The transmitted energy is measured by placing the sample between lens and the focal point. Thereafter the sample is moved in small steps towards and beyond the focus, and the transmission is measured at each position. The laser intensity appears to be maximum at the focus and the sample experiences different laser intensities on either side of the focus. The graph plotted between position z and the normalized transmittance of the sample is known as the open-aperture z-scan curve. Fig.16 reveals the nature of the absorptive nonlinearity in the system. If a spatially Gaussian laser beam is used for excitation, then each z-position will correspond to an input laser energy density (fluence) of $4(\ln 2)^{1/2}Ein/\pi^{3/2}\omega(z)^2$, where E_{in} is the input laser pulse energy and ω(z) is the beam radius. ω (z) is given by $\omega(0)*[1+(z/z_0)^2]^{1/2}$, where ω(0) is the beam radius at the focus and $z_0 = \pi\omega(0)^2/\lambda$ is the Rayleigh range (diffraction length), where λ is the excitation wavelength. Using the data of input laser fluence and the sample transmission it is possible to plot nonlinear transmission curve.

We used a planoconvex lens of 20 cm focal length for focusing the laser. The solution taken in a 1 mm thick glass cuvette (Hellma GmBH) had a linear transmission of 88% after surface reflection losses. The cuvette was mounted on a programmable linear translation stage. The input energy reaching the sample and the energy transmitted by the sample were measured using two pyroelectric energy probes (RjP 735, Laser Probe Inc.). The interval between successive laser pulses was large enough (about 1 s) to allow complete thermal relaxation of the sample between adjacent laser pulses. The experiment was automated using a Labview program running in the Windows XP Environment. The experimental details and the results observed are given in the Table 5.

Fig.16 and Fig.17 shows the open aperture z-scan fit and the optical limiting curve of ATCC respectively. Upon trying nonlinear transmission equations for two-photon and three-photon absorptions, the open-aperture z-scan data is found

to fit well to the three-photon absorption (3PA) process, given by the equation 6.1 [23]

$$T = \frac{(1-R)^2 \exp(-\alpha L)}{\sqrt{\pi}\, p_0} \int_{-\infty}^{\infty} \ln[\sqrt{1 + p_0{}^2 \exp(-2\tau^2)} + p_0 \exp(-\tau^2)] d\tau \quad \ldots\ldots\ldots\ldots \quad (6.1)$$

Where T is the measured transmission of the sample, L and R are the sample length and surface reflectivity respectively, and α is the linear absorption coefficient. p_0 in eqn.3.1 is given by $p_0 = \sqrt{2\gamma(1-R)^2 I_0{}^2 L_{eff}^{`}}$ where $I_0$ is the on-axis peak intensity, $L`_{eff}$ is given by [1-exp(-2αL)]/2α, and γ is the three-photon absorption coefficient. The numerically calculated effective three photon absorption coefficient (γ_{eff}) is found to be $4499 \times 10^{12} m^3/W^2$. The results are given in the Table 6.

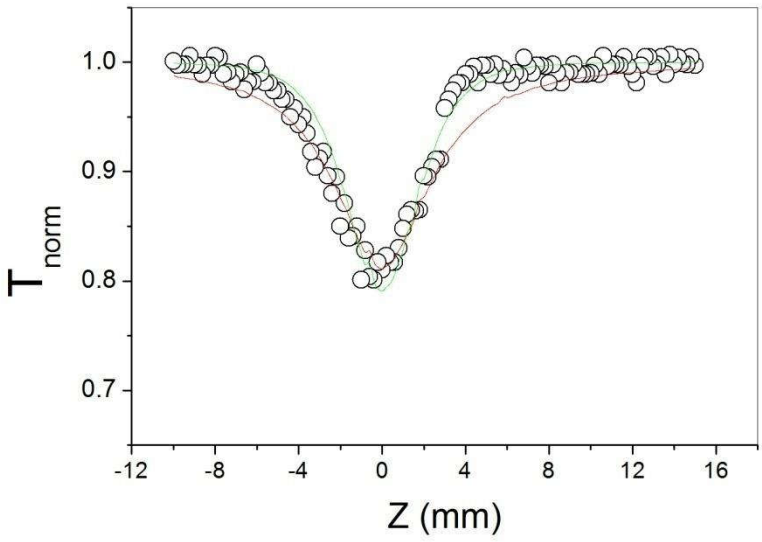

Fig. 16: *Open aperture z scan curve of ATCC*

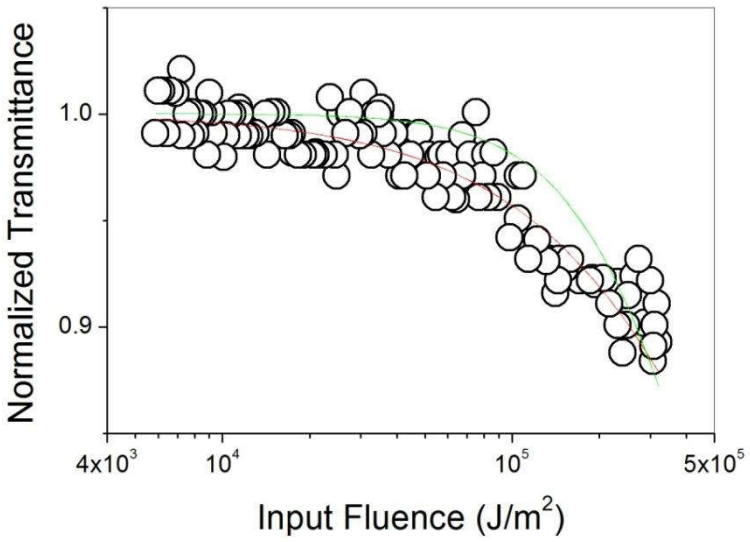

Fig.17: *Non linear transmission curve of the ATCC*

Table 6: *The Open aperture Z-scan Experimental Details of ATCC*

Wavelength (nm)	Pulse width (ps)	Average Energy (micro joule)	Two Photon absorption coefficient(β) (m/W)	Three photon absorption coefficient (γ) (m^3/w^2)	Linear Transmission
532.00	4999.99	244.68	$10x10^{-12}$	$4499X\ 10^{-12}$	0.870000

4.0 Conclusion.

Good quality crystals of ATCC are grown by slow evaporation technique and the molecular structure of the compound were confirmed. The single crystal X-ray studies gives the unit cell parameters of the crystal and the HRXRD study reveals that the quality of the grown crystal is good and it may be suitable for photonics applications. Optical transmission region and band gap of the material is determined using Uv-visible absorption studies. The SEM picture of the crystal gives the surface morphology of the ATCC crystal. It is found that both dielectric constant and dielectric loss of the ATCC crystal decreases with increasing frequency. The ac conductivity measurements were carried out and the measured value of conductivity is found to increase with temperature. The Piezoelectric charge coefficient was measured and hysteresis loop, of the ATCC crystal has been traced using PE loop tracer and loop parameters such as remnant polarization (P_r) and coercive field (E_c) were measured. The grown crystals are also subjected to Photoconductivity studies using the Keithley 6485 Pico ammeter and the field dependence of conductivity was measured. Open aperture Z scan curve fitted and the three photon absorption coefficient is calculated.

5. References

1. V. Siva shankar, R. Sankar, R. Siddheswaran, R. Jayavel, P. Murugakoothan., Material Chemistry and Physics 109(2008) 119.
2. N.J. Long, Angew., Chem. Int. Ed. Engl. 34(1995) 21.
3. M. Jiang, Q. Fang, Adv. Mater. 11 (**1999**) 1147.
4. Hou Wenbo, Yuan Duorong, Xu Dong, Zhang Nan, Yu Wentao, Liu Mingguo, Tao Xutang, Sun Suoyang and Jiang Minhua., Journal of Crystal Growth 133(1993) 71
5. H L Bhat, Bull, matt, sci. Vol.17, No.7 December 1994, 1223-1249.
6. H.Q. Sun, D.R. Yuan, X.Q. Wang, Y.Q. Lu, Z.H. Sun, X.C. Wei, X.L. Duan, C.N. Luan, M.K. Lu, D. Xu., J.Crystal Growth 256(2003) 183
7. N. Zhang, M.H. Jaing, D.R. Yuan, D. Xu, X.T. Tao., Chin. Physics. Lett. 6(1989)280.
8. N. Zhang, M.H. Jaing, D.R. Yuan, D. Xu, X.T. Tao and Z.S. Shao., Jornal of Crystal Growth 102(1990) 581.
9. H.Q. Sun, D.R. Yuan, X.Q. Wang, Y.Q. Lu, Z.H. Sun, X.C. Wei, X.L. Duan, C.N. Luan, M.K. Lu, D. Xu., J.Crystal Growth 256(2003) 184.
10. Ginson P.Joseph, K. Rajarajan, M. Vimalan, S.Selvakumar, S.M. Ravi Kumar, J.Madhavan, P. Sagayaraj., Material Research Bulletin 42(2007) 2041.
11. R. Perumal and S. Moorthy Babu, J. Crystal Growth 310 (**2008**) 2050.
12. R. Josephine Usha et al Arch. Appl. Sci. Res., 2012, 4 (3):1266-1273.
13. M. Jose, B. Sridhar, G. Bhagavannarayana, K. Sugandhi, R.Uthrakumar, C. Justin Raj, D. Tamilvendhan, S.Jerome Das, J.Crystal Growth 312 (**2010**) 793.
14. P. Anandan, T. Saravanan, S. Vasudevan, R. Mohan Kumar, R. Jayavel, J. Crystal Growth 312 (2010) 837.
15. W.B. Hou, Z.H. Yang, M.G. Liu, D.R. Yuan, D. Xu, N. Zhang, W.T. Yu,Y.H. Bing, S.Y. Sun, X.T. Tao, M.H. Jiang, Mater. Lett. 18 (1994) 207.
16. Tauc J., (1974), 'Amorphous and liquid semiconductors', J Tauc Ed. Plenum, New York.
17. R. Perumal and S. Moorthy Babu, Mat. Chem and Phys. 107 (2008) 23.
18. L.R. Dalton, J. Phys. Condens. Matter. 15 (2003) R897.
19. S.I. Bhat, P.M. Rao, A.P.G. Bhat, D.K. Avasthi, Surf. Coat. Technol. 58 (2002) 725–728.
20. A.K. Jonscher, Nature 267 (1977) 673.
21. V.N. Joshi, Photoconductivity, Marcel Dekker, New York, 1990.
22. Sheik-Bahae M, Said A A, Wei T M, Hagan D J and Van-Stryland E W 1990 IEEE J. Quantum Electron. 26, 760.
23. R.L. Sutherland, Handbook of Nonlinear Optics (Dekker, New York, 1996).